ACS APPLIED MATERIALS & INTERFACES

RESEARCH ARTICLE

www.acsami.org

Construction of TiO_2 Hierarchical Nanostructures from Nanocrystals and Their Photocatalytic Properties

Tiejian Zhu, Jing Li, and Qingsheng Wu*

Department of Chemistry, Tongji University, Shanghai, 200092, People's Republic of China

Supporting Information

ABSTRACT: Anatase TiO_2 mesoporous structures with high specific surface areas are of special significance in various applications. In this work, hierarchical anatase TiO_2 materials with flowerlike morphologies have been prepared via a one-step template-free hydrothermal method, by using titanocene dichloride as precursor and EDA as chelating agent in aqueous solution. Particularly, the hierarchical structures are assembled from very thin TiO_2 nanosheets, which are composed of numerous highly crystallized anatase nanocrystals. In addition, the assembled materials own relatively large specific surface areas of 170 m^2/g, and uniform mesopores of 7 nm. We further demonstrate that the hierarchical TiO_2 materials show very good photocatalytic performance when applied in photodegradation of methylene blue, which should be related to the unique features of hierarchical structures, large specific surface areas and high crystallization degree of the obtained TiO_2 materials. With these features, the hierarchical TiO_2 may find more potential applications in the fields such as dye-sensitized solar cells and lithium ion batteries.

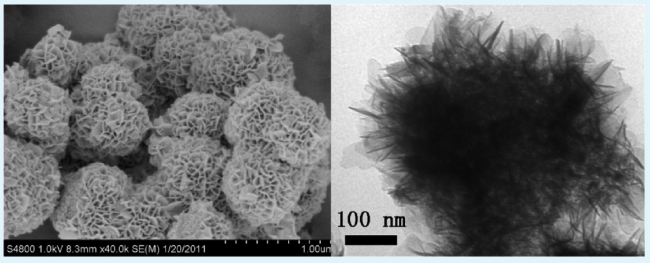

KEYWORDS: TiO_2, anatase, titanocene dichloride, hierarchical, photocatalytic, hydrothermal

INTRODUCTION

It is widely recognized that properties and performances of nanomaterials are highly related to their controlled morphologies, sizes, and structures.[1−5] Particularly, to construct inorganic nanomaterials into 3D hierarchical structures have attracted significant research interests in recent years, because of their potential applications in adsorption, separation, photocatalysis, biology, electronics, sensor, dye-sensitized solar cell, and lithium ion storages.[6−15] A range of methods are now available to construct these structures, of which one-pot template-free hydrothermal/solvothermal routes are more recommendable than the template ones, due to their simple operation procedures and easily adjustable process parameters. For most one-pot syntheses, the formation of hierarchical structure experiences three steps: the nucleation of seeds, further growth of nanobuilding units, and assembly of them in certain manners under the assistance of various interactions. The typical building blocks could be nanoparticles (0D),[16] nanorods/nanotubes (1D)[17,18] or very thin nanosheets/nanoplates (2D),[14,19] whereas the finally achieved structures largely vary in morphologies from spheres, hollow spheres to flowerlike ones, etc.[16,17,20]

Especially, flowerlike hierarchical nanostructures organized from 1D or 2D nanobuilding units are found to be attractive photocatalyst materials. On the one hand, they own the advantages of enhanced light absorption, as a result of multireflection within the numerous voids of the materials, thus usually exhibiting higher photo efficiency.[21−23] On the other hand, the assembled nanostructures provide much more exposed surface region, well facilitating the adsorption and photoreaction of reactants. Till now, many inorganic photocatalytic materials are able to be prepared in flower like hierarchical structures, such as Bi_2WO_6,[24] Bi_2MoO_6,[25] ZnO,[21,26,27] CeO_2,[28] and BiOX (X = Cl, Br, I).[29,30]

As a classical and important photocatalyst material, TiO_2 has been extensively investigated. Very recently several groups reported flower-like hierarchical TiO_2 with quite special photocatalytic activities.[31−34] For instance, Zheng et al.[34] prepared the hierarchical TiO_2 microspheres built from nanotubes, which show specific area as high as 300 m^2/g and good degradation ability to methyl orange. But this preparation adopted a top-down strategy in which two step hydrothermal reactions are required. Two other works[31,32] achieved flowerlike hierarchical TiO_2 nanostructures by applying the facile one-pot assembly routes, which also show good photocatalytic activities, but the specific surface areas are relatively low (around 70 m^2/g). Therefore, it is highly desirable to develop an easy synthetic process for hierarchical TiO_2 nanostructures with high specific surface areas and good photocatalytic performances.

In this work, we report an aqueous preparation approach for flowerlike hierarchical TiO_2 nanostructures by using a one-pot, template-free hydrothermal method. Different from the commonly used precursor species titanium tetrachloride/fluoride/isopropoxide and tetrabutyl titanate, titanocene dichloride was chosen in our reaction system. Titanocene dichloride, a type of metalorganic complex, is widely recognized for its antitumor

Received: May 27, 2011
Accepted: July 29, 2011
Published: July 29, 2011

properties.[35] In our present synthesis, this precursor reveals the advantages of better control of the reaction rate and thus the product morphology. With a simple hydrothermal reaction of titanocene dichloride with ethylenediamine in aqueous solution, we have acquired flowerlike hierarchical TiO_2 spheres assembled from amorphous nanosheets. After a mild calcination process, the amorphous nanosheets are transferred to highly crystalline ones, composed of numerous TiO_2 nanoparticles. Interestingly, the assembled materials own relatively large specific surface areas of 170 m^2/g, even comparable to the ordered mesoporous TiO_2 obtained from soft-templating route.[36] Furthermore, we tested their photodegradation capability to methylene blue, which indeed shows higher activities than the commercial TiO_2 product.

EXPERIMENTAL SECTION

The flowerlike hierarchical TiO_2 nanostructures were synthesized from hydrolysis of titanocene dichloride ($Ti(Cp)_2Cl_2$), with ethylenediamine (EDA) as chelating agent. In a typical preparation, 20 mg of $Ti(Cp)_2Cl_2$ was dispersed into 10 mL of deionized water, to which 2 drops of EDA was further added. The mixture was sonicated for 10 min and transferred to a Teflon-lined stainless steel autoclave with 20 mL capacity. Hydrothermal synthesis was then conducted at 120 °C for 1−12 h in an electric oven. After the reaction, the resultant hierarchical TiO_2 nanomaterials were washed thoroughly with ethanol and water. It should be mentioned that the TiO_2 products obtained at this step were amorphous and mixed with some carbon impurity. To remove the carbon from the sample and simultaneously achieve highly crystalline pure TiO_2 products, the as-prepared samples were calcined at 400 °C for 2 h in air to get the final products.

In photocatalytic testing, 40 mg of the obtained catalyst was dispersed in 50 mL of methylene blue (MB) solution with a concentration of 20 mg/L and the photoreaction was conducted under continuous stirring. A 300 W Hg lamp cooled with a water jacket was used as the irradiation source and placed 30 cm apart from the reactor. After each reaction, the solution was separated from catalyst by centrifugation. The concentration of MB was measured with a UV−vis spectrophotometer (Agilent 8453) and the absorbance at 656 nm was monitored.

MATERIALS CHARACTERIZATION

The crystallographic structure of the solid samples was determined with X-ray diffraction (XRD, Bruker D8) with Cu Kα radiation (λ = 0.154056 nm) (Germany), using a voltage of 40 kV, a current of 40 mA, and a scanning rate of 0.02°/s, in 2θ ranges from 10° to 70°. The spatial and morphological studies were carried out with field-emission scanning electron microscopy (FESEM, Hitachi S4800) at an accelerating voltage of 1−5 kV and transmission electron microscopy (TEM, JEM2010) at an accelerating voltage of 200 kV. Thermogravimetric analysis (TGA, STA 409PC, NETZSCH) was carried out under a flow of air. Approximately 10 mg of the sample was loaded into a standard Al_2O_3 crucible, which was heated from room temperature to 1000 °C at a heating rate of 10 °C/min. N_2 adsorption−desorption measurements were conducted on a Micromeritcs Tristar 3000 analyzer at 77 K. Before the actual measurements, the sample was degassed at 150 °C for 6 h. Brunauer−Emmett−Teller (BET) surface area was determined using adsorption data. Pore size distribution was achieved through Barrett−Joyner−Halenda (BJH) method. UV−vis diffuse reflectance spectra were measured at room temperature with a UV−vis spectrometer (BWS002, BWTEK).

RESULTS AND DISCUSSION

The crystal structures of the obtained TiO_2 products were investigated with XRD method. Because our reactants only consist

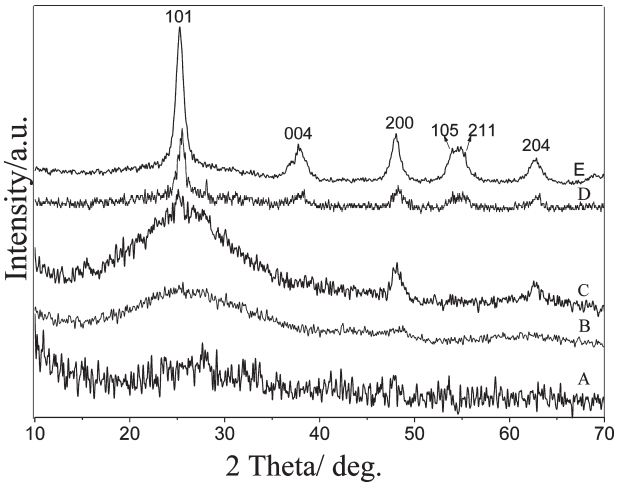

Figure 1. XRD patterns for the hierarchical TiO_2 samples synthesized at 120 °C for (A) 1, (B) 6, and (C) 12 h. (D, E) Sample B calcined at 350 and 400 °C for 2 h.

of titanocene dichloride and water, together with a little amount of EDA, it is unsuspicious that a hydrolysis reaction of titanocene dichloride occurred in the hydrothermal process and TiO_2 could be made as a main solid product. As shown in Figure 1, the samples prepared with relatively short reaction time of 1 and 6 h show no distinct diffraction peaks, indicating the amorphous or poorly crystalline TiO_2. For the sample synthesized from 12 h of aging time, one can find three diffraction peaks, able to be ascribed to 101, 200, and 204 faces of the tetragonal anatase TiO_2 (SG: $I4_1/amd$; a_0 = 3.79 Å and c_0 = 9.51 Å; JCPDS No. 21−1272), which is a result of partly crystallized TiO_2 product. In addition, from all three patterns for the samples obtained after hydrothermal reaction but before calcinations, an obvious hump at 2θ from 20 to 35° can be detected. It demonstrates the existence of carbon in the sample, and is in agreement with the observation of gray color product. Carbon is produced from decomposition of cyclopentadiene rings included in the precursor titanocene, as that happened to ferrocene in a hydrolysis process.[37] In our present synthesis, carbon is just a byproduct which can be removed by a simple calcination treatment. As indicated by the XRD patterns (Figure 1D,E), after calcinations, the hump disappears (simultaneously, the samples change to white color), confirming the removal of impurity carbon from the product. On the other hand, the six resolved peaks well assign the sample to anatase TiO_2, showing that the product is highly crystallized and phase pure. The diffraction peaks for the sample calcined at 400 °C are more resolved than those calcined at 350 °C, implying the higher crystallization degree at a higher temperature. Besides, crystalline particles for the calcined products are relatively small in sizes, as indicated by the broadened diffraction peaks.

TGA (Figure 2) measurement for the as prepared sample reveals two weight loss regions. The weight loss of 5% below 120 °C could be ascribed to the evaporation of free water included in the porous structures, whereas the weight loss of 10% at higher temperature range should be due to the existence of organic species.

SEM images in Figure 3 show the morphological evolution of the as-prepared TiO_2 samples. At a short reaction time of 1 h, TiO_2 displays the sphere and slightly aggregated sphere morphology

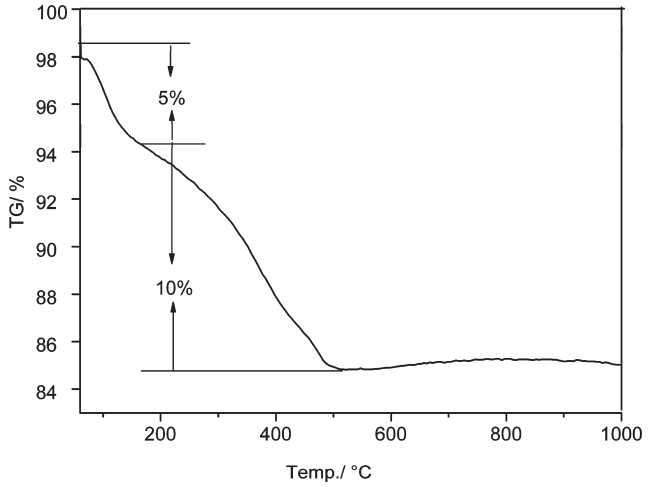

Figure 2. TG curve for the hierarchical TiO_2 sample synthesized at 120 °C for 6 h.

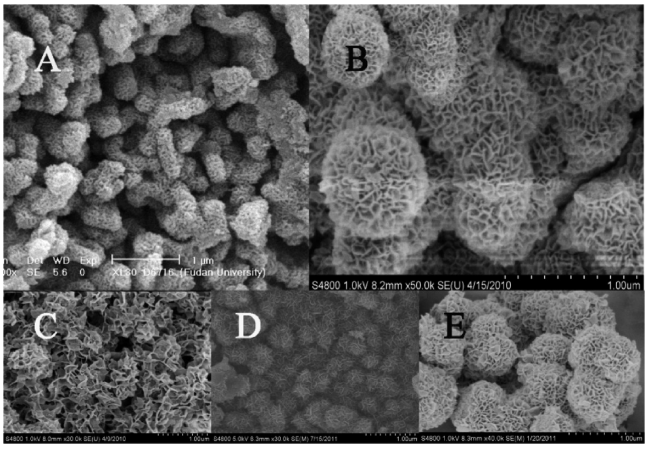

Figure 3. SEM images of the hierarchical TiO_2 samples synthesized at 120 °C for (A) 1, (B) 6, and (C) 12 h. (D, E) Sample B calcined for 2 h at 350 and 400 °C, respectively.

with the sizes of around 350 nm. Particularly, the spheres are in hierarchical structures, which are organized from thin nanosheets in an interwoven style. When aging time is prolonged to 6 h, the hierarchical TiO_2 keeps the sphere morphologies, while the sizes increase to about 650 nm. Furthermore, it can be observed from Figure 3B that the nanosheets exhibit relatively loose stacking compared to those prepared under 1 h reaction. The products obtained from 12 h reaction are even looser, as shown in Figure 3C, from which the assembled spheres almost collapse. Hence, it is supposed that the hydrolysis reaction of titanocene dichloride first forms amorphous TiO_2 nanosheets (see XRD results before), which quickly self-assemble into hierarchical structures under the assistance of van der Waals interactions. With prolonged reaction duration, the nanosheets further grow, which induces larger sizes of the spheres. As a result, the voids become to be more evident. When the hierarchical spheres continuously grow with even longer time (more than 12 h), the nanosheets become larger with partly crystallized anatase phase, in which the torsional stresses exceed van der Waals interactions for assembling the nanosheets. As a result, the nanosheets separate from each other. After a calcination treatment at 350

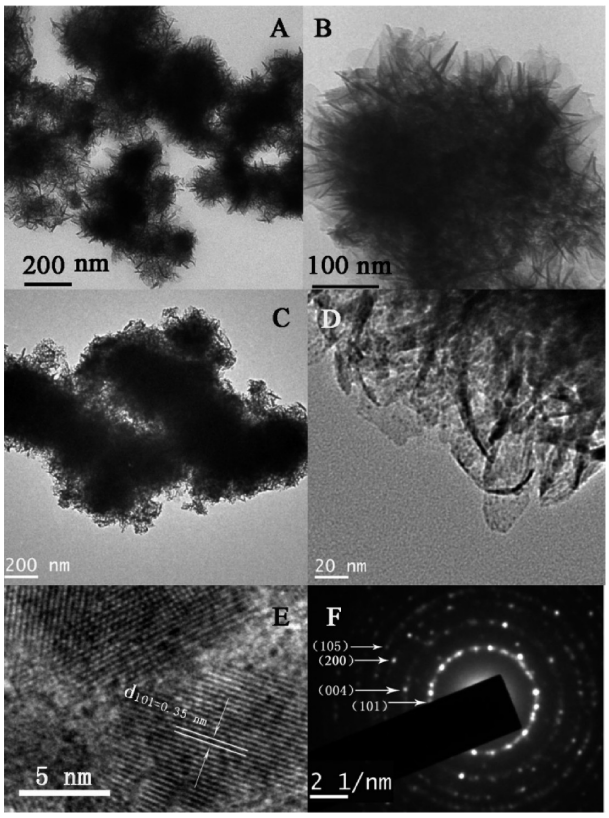

Figure 4. (A, B) TEM images of the TiO_2 sample synthesized at 120 °C for 6 h; (C, D) TEM images, (E) HRTEM, and (F) SAED pattern of the TiO_2 sample A after calcination at 400 °C for 2 h.

and 400 °C for 2 h, the as-prepared amorphous TiO_2 samples were transferred into crystalline ones, which well-preserve the spherical morphology and hierarchical structures (Figure 3D,E).

TEM technique is used to examine the detailed morphologies and structures of the TiO_2 samples. From images A and B Figure 4, as-made TiO_2 shows that hierarchical structures are in flowerlike shapes, and assembled from numerous nanosheets, similar with the SEM observation. Especially, the nanosheets have very thin thickness of about several nanometers, and relatively large wideness of dozens of nanometers. According to XRD analysis, these nanosheets could be composed of amorphous TiO_2 species. After calcination process, the crystallized sample well preserves the flowerlike morphologies and the hierarchical structures, as indicated in images C and D in Figure 4. Simultaneously, it is found that the TiO_2 nanosheets are transferred into polycrystalline ones, consisted of numerous well-crystallized nanoparticles with sizes around 6 nm (Figure 4D,E). Particularly, in the HRTEM image (Figure 4E), (101) crystalline planes of TiO_2 with an interplanar spacing of 0.35 nm can be clearly observed.[38] The SAED pattern (Figure 4F) also confirms the polycrystalline nanosheets, and the most distinct four concentric diffraction rings can be assigned to (101), (004), (200), and (105) planes of the anatase TiO_2 from the center.[39]

N_2 adsorption−desorption isotherms (Figure 5) of the hierarchical TiO_2 structures are also measured. All the as-prepared and calcined samples exhibit typical type-IV isotherms and type H3 hysteresis loops, indicating the existence of mesopores. The pore sizes for the samples obtained without calcinations are 12 nm (1 h), 10 nm (6 h) and 10 nm (12 h), respectively. The product

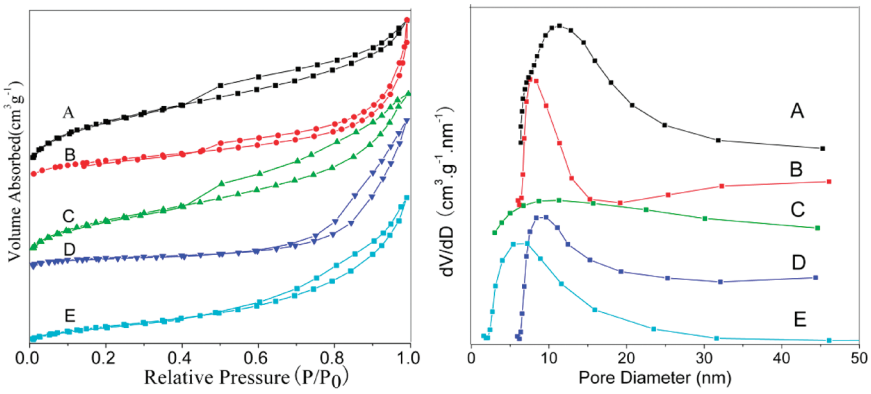

Figure 5. N_2 adsorption−desorption isotherms (left) and pore size distribution plots (right) of the hierarchical TiO_2 samples synthesized at 120 °C for (A) 1, (B) 6, and (C) 12 h. (D, E) Sample B calcined for 2 h at 350 and 400 °C, respectively.

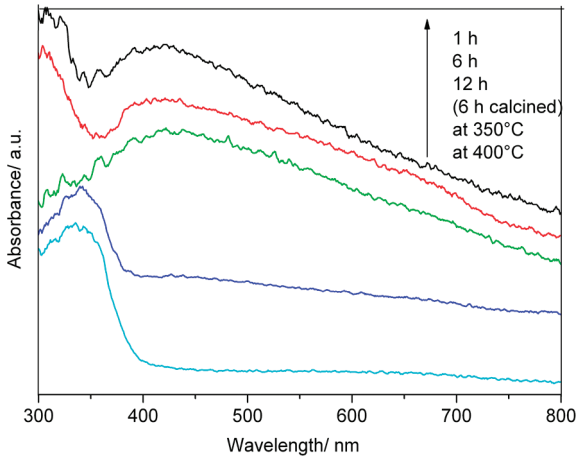

Figure 6. UV−vis diffuse reflectance spectra of TiO_2 hierarchical structures under different reaction conditions.

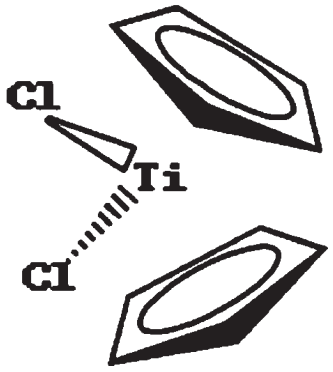

Figure 7. Structure of titanocene dichloride.

calcined at 350 °C shows pore size of about 10.5 nm, similar with the untreated sample, revealing negligible framework shrinkage. But a higher calcination temperature (400 °C) induces the smaller size of 7 nm, a result of visible framework shrinkage of mesoporous materials during calcination process. At the same time, the specific surface areas are 413 m^2 /g (1 h), 340 m^2 /g (6 h) and 420 m^2 /g (12 h) respectively, for the uncalcined TiO_2 products. While after calcinations, the sample calcined at 400 °C has smaller specific surface area, 170 m^2 /g. This big difference is because that carbon impurity is included in the as-prepared samples, which provides copious micropores to the materials. After calcinations, carbon is removed and the products are phase-pure mesoporous TiO_2. Indeed, the value of 170 m^2 /g is much higher than the reported similar structures for TiO_2 materials.[31,32] A possible explanation to this high specific surface area is that removal of the carbon impurities makes additional mesopores to the TiO_2, apart from those resulted from stacking of nanosheets.

The light absorption characteristics of the TiO_2 products are characterized using UV−vis diffuse reflectance spectra (Figure 6). The three samples obtained from 1, 6, and 12 h of hydrothermal reactions show continuous adsorption in the full spectrum band. This is due to certain amount of carbon is involved in the samples.[40,41] After calcination treatment, the two phase-pure TiO_2 products show typical TiO_2 absorption characteristics, with the absorption edges located at 410 nm.

On the basis of the above materials characterization, we would address some important points for the formation of nanosheet based TiO_2 hierarchical structures. The precursor adopted in this work is titanocene dichloride (Figure 7), a substance widely used as metalorganic complex, but few applied in production of TiO_2. Because of the existence of the two cyclopentadiene rings in the molecules, their hydrolysis rate should be slower than the species such as $TiCl_4$, a beneficial factor to morphology control of the nanomaterials. In addition, a trace amount of EDA is also very important to the present preparation. Indeed, if no EDA is added in the precursor solution, one can only get the tiny nanoparticles but not the hierarchical structures (Figure S1). It is supposed that some new titanium complexes might be formed under the existence of EDA.[42] The nucleation, growth, and assembly of the TiO_2 hierarchical structures should be related to the steric hindrance of the new complexes in the reaction solution, and adsorption and deactivation of the ligand EDA on the growing part of the product.

For the flowerlike hierarchical TiO_2 materials achieved in this work, we evaluated their photocatalytic activity by photodegradating methylene blue. As shown in Figure 8, before the irradiation, the reaction system was continuously stirred for 4 h to reach the adsorption balance.[43] The as-prepared samples obtained from 6 and 12 h of hydrothermal reactions show distinct adsorption (12 mg/g), which is understandable since the samples contain some carbon species and possess relatively large specific surface areas. Furthermore, the former has no any photodegradation

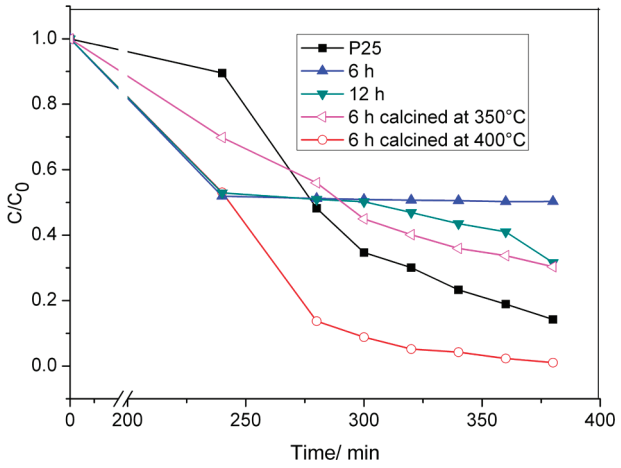

Figure 8. Photocatalytic conversions of methylene blue using the hierarchical TiO_2 samples obtained at different reaction conditions. TiO_2 P25 from Degussa Company is used as a reference.

ability to methylene blue, and the latter display a little. It is expected since they are amorphous and poorly crystallized products. The adsorption amount for the calcined sample at 400 °C is also as high as 12 mg/g, about 4.8 times higher than that of P25 (2.5 mg/g). It should be due to its larger specific surface area than that of P25 ($S_{BET} \approx 45$ m^2/g). In addition, upon irradiation, this anatase TiO_2 product also shows a distinctly rapider degradation rate (0.0363 min^{-1}) than that of P25 (0.0159 min^{-1}), a mixed phase of anatase and rutile. One reason might be attributed to more reaction sites created by larger surface area of TiO_2 flower and the mesoporous channels inside the materials. And another reason should be ascribed to phase pure anatase and better crystallization degree of our prepared hierarchical TiO_2, as it is well-known that photocatalytic property is greatly related to the crystallization degree of anatase. Actually, in this test the sample calcined at 350 °C shows slower degradation speed (0.0125 min^{-1}) than that of P25, which should be partly ascribed to their lower crystallization degree (Figure 1D). The above results clearly show that the hierarchical anatase TiO_2 material with mesoporous structures synthesized in this work is an excellent photocatalyst material.

CONCLUSION

In summary, a simple one-pot approach for preparation of flowerlike hierarchical TiO_2 nanostructures has been presented. The hierarchical product shows a mesoporous structure with a high specific surface area of 170 m^2/g and relatively narrow pore size distribution of 7 nm. The synergetic effects of the specially chosen titanocene dichloride precursor and ligand EDA are affordable to the assembly of the hierarchical structures. Furthermore, we have illustrated that the hierarchical TiO_2 material displays good performance in the photocatalytic reaction, a result of large specific surface area, mesoporous structures, and high crystallization degree of anatase. With these features, the hierarchical TiO_2 may find more potential applications in the fields such as dye-sensitized solar cells and lithium ion batteries.

ASSOCIATED CONTENT

Supporting Information. TEM image for the TiO_2 product obtained without EDA added in the precursor solution. This material is available free of charge via the Internet at http://pubs.acs.org/.

AUTHOR INFORMATION

Corresponding Author
*E-mail: qswu@tongji.edu.cn.

ACKNOWLEDGMENT

The authors are grateful for the financial support of the National Natural Science Foundation (51072134) of China, the State Major Research Plan (973) of China (2011CB932404), the Shanghai Key Laboratory of Molecular Catalysis and Innovative Materials (2012MCIMKF03), and ChangJiang Delta Union Project (10140702017).

REFERENCES

(1) Feng, Y. C.; Li, L.; Ge, M.; Guo, C. S.; Wang, J. F.; Liu, Lu. *ACS Appl. Mater. Interface* **2010**, *2*, 3134–3140.
(2) Krins, N.; Faustini, M.; Louis, B.; Grosso, D. *Chem. Mater.* **2010**, *22*, 6218–6220.
(3) Rawolle, M.; Ruderer, M. A.; Prams, S. M.; Zhong, Q.; Magerl, D.; Perlich, J.; Roth, S. V.; Lellig, P.; Gutmann, J. S.; Müller-Buschbaum, P. *Small* **2011**, *7*, 884–891.
(4) Orilall, C. M.; Abrams, N. M.; Lee, J.; DiSalvo, F. J.; Wiesner, U. J. *Am. Chem. Soc.* **2008**, *130*, 8882–8883.
(5) Docampo, P.; Guldin, S.; Stefik, M.; Tiwana, P.; Orilall, M. C.; Hüttner, S.; Sai, H.; Wiesner, U.; Steiner, U.; Snaith, H. J. *Adv. Funct. Mater.* **2010**, *20*, 1787–1796.
(6) Bao, N.; Li, Y.; Wei, Z. T.; Yin, G. B.; Niu, J. J. *J. Phys. Chem. C* **2011**, *115*, 5708–5719.
(7) Masuda, Y.; Ohji, T.; Kato, K. *Cryst. Growth Des.* **2010**, *10*, 913–922.
(8) Yang, X. F.; Jin, C. J.; Liang, C. L.; Chen, D. H.; Wu, M. G.; Yu, J. C. *Chem. Commun.* **2011**, *47*, 1184–1186.
(9) Lü, X. J.; Huang, F. Q.; Mou, X. L.; Wang, Y. M.; Xu, F. F. *Adv. Mater.* **2010**, *22*, 3719–3722.
(10) Yang, W. G.; Li, J. M.; Wang, Y. L.; Zhu, F.; Shi, W. M.; Wan, F. R.; Xu, D. S. *Chem. Commun.* **2011**, *47*, 1809–1811.
(11) Shang, M.; Wang, W. Z.; Yin, W. Z.; Ren, J.; Sun, S. M.; Zhang, L. *Chem.—Eur. J.* **2010**, *16*, 11412–11419.
(12) Guan, X. F.; Li, L. P.; Li, G. S.; Fu, Z. W.; Zheng, J.; Yan, T. J. *J. Alloys Compd.* **2011**, *509*, 3367–3374.
(13) Zhu, J.; Wang, S. H.; Wang, J. G.; Zhang, D. Q.; Li, H. X. *Appl. Catal. B: Environ.* **2011**, *102*, 120–125.
(14) Wang, C. X.; Yin, L. W.; Zhang, L. Y.; Qi, Y. X.; Lun, N.; Liu, N. N. *Langmuir* **2010**, *26*, 12841–12848.
(15) Chen, J. S.; Tan, Y. L.; Li, C. M.; Cheah, Y. L.; Luan, D. Y.; Madhavi, S.; Chiang, F. Y. B.; Archer, L. A.; Lou, X. W. *J. Am. Chem. Soc.* **2010**, *132*, 6124–6130.
(16) Zhang, L. Z.; Yu, J. C. *Chem. Commun.* **2003**, 2078–2079.
(17) Guan, X. F.; Li, L. P.; Li, G. S.; Fu, Z. W.; Zheng, J.; Yan, T. J. *J. Alloys. Compd.* **2011**, *509*, 3367–3374.
(18) Tang, Y. F.; Yang, L.; Chen, J. Z.; Qiu, Z. *Langmuir* **2010**, *26*, 10111–10114.
(19) Zhu, J.; Wang, S. H.; Bian, Z. F.; Cai, C. L.; Li, H. X. *Res. Chem. Intermed.* **2009**, *35*, 769–777.
(20) Jiao, Y. Z.; Peng, C. X.; Guo, F. F.; Bao, Z. H.; Yang, J. H.; Lukas, S. M.; Ricky, D.; Qin, Y.; Deng, Z. F. *J. Phys. Chem. C* **2011**, *115*, 6405–6049.
(21) Liu, S. W.; Li, C.; Yu, J. G.; Xiang, Q. J. *CrystEngComm.* **2011**, *13*, 2533–2541.
(22) Liu, S. W.; Yu, J. G. *J. Solid State Chem.* **2008**, *181*, 1048–1055.
(23) Han, W. Q.; Wu, L. J.; Klie, R. F.; Zhu, Y. M. *Adv. Mater.* **2007**, *19*, 2525–2529.

(24) Zhang, L. S.; Wang, W. Z.; Chen, Z. G.; Zhou, L.; Xu, H. L.; Zhu, W. *J. Mater. Chem.* **2007**, *17*, 2526–2532.
(25) Tian, G. H.; Chen, Y. J.; Zhou, W.; Pan, K.; Dong, Y. Z.; Tian, C. G.; Fu, H. G. *J. Mater. Chem.* **2011**, *21*, 887–892.
(26) Lu, H. B.; Wang, S. M.; Zhao, L.; Li, J. C.; Dong, B. H.; Xu, Z. X. *J. Mater. Chem.* **2011**, *21*, 4228–4234.
(27) Lu, F.; Cai, W. P.; Zhang, Y. G. *Adv. Funct. Mater.* **2008**, *18*, 1047–1056.
(28) Zhang, H.; Li, H. F.; Li, W.; Meng, S. L.; Li, D. Q. *J. Colloid Interface Sci.* **2009**, *333*, 764–770.
(29) Song, J. M.; Mao, C. J.; Niu, H. L.; Shen, Y. H.; Zhang, S. Y. *CrystEngComm.* **2010**, *12*, 3875–3881.
(30) Zhang, X.; Ai, Z. H.; Jia, F. L.; Zhang, L. Z. *J. Phys. Chem. C* **2008**, *112*, 747–753.
(31) Duong, T.; Phan, N.; Kim, E. J.; Hahn, S. H.; Kim, W. J.; Shin, E. W. *J. Colloid Interface Sci.* **2011**, *356*, 138–144.
(32) Tian, G. H.; Chen, Y. J.; Zhou, W.; Pan, K.; Tian, C. G.; Huang, X. R.; Fu, H. G. *CrystEngComm.* **2011**, *13*, 2994–3000.
(33) Ho, W. K.; Yu, Jimmy C.; Lee, S. C. *Chem. Commun.* **2006**, 1115–1117.
(34) Zheng, Z. K.; Huang, B. B.; Qin, X. Y.; Zhang, X. Y.; Dai, Y. *Chem.—Eur. J.* **2010**, *16*, 11266–11270.
(35) Meléndez, E. *Crit. Rev. Oncol. Hemat.* **2002**, *42*, 309–315.
(36) Zhang, J. Y.; Deng, Y. H.; Gu, D.; Wang, S. T.; She, L.; Che, R. C.; Wang, Z. S.; Tu, B.; Xie, S. H.; Zhao, D. Y. *Adv. Energy Mater.* **2011**, *1*, 241–248.
(37) Yuan, P. S.; Wu, Q. S.; Ding, Y. P.; Wu, H. Q.; Yang, X. C. *Carbon* **2009**, *47*, 2648–2654.
(38) Cao, F. F.; Wu, X. L.; Xin, S.; Guo, Y. G.; Wan, L. J. *J. Phys. Chem. C* **2010**, *114*, 10308–10313.
(39) Zhang, W.; Zhu, R.; Ke, L.; Liu, X. H.; Liu, B.; Seeram, R. *Small* **2010**, *6*, 2176–2182.
(40) Zhang, L. X.; Liu, P.; Su, Z. X. *J. Mol. Catal. A: Chem.* **2006**, *248*, 189–197.
(41) Wang, H. Q.; Wu, Z. B.; Liu, Y. *J. Phys. Chem. C* **2009**, *113*, 13317–13324.
(42) Chang, Y.; Lye, M. L.; Zeng, H. C. *Langmuir* **2005**, *21*, 3746–3748.
(43) Zhang, R. Y.; Tu, B.; Zhao, D. Y. *Chem.—Eur. J.* **2010**, *16*, 9977–9981.